Analyst

ROYAL SOCIETY OF CHEMISTRY

PAPER

View Article Online
View Journal | View Issue

Cite this: *Analyst*, 2026, **151**, 1657

Sustainable, biodegradable paper sensor functionalized with oxidised bis(indolyl)methane for temporal discrimination of hazardous organophosphorus simulants in aqueous media

Rikitha S. Fernandes and Nilanjan Dey *

Organophosphorus (OP) nerve agents pose significant threats to human health, chemical warfare scenarios, and biomarker-based exposure assessment, necessitating rapid, selective, and field-deployable detection strategies. Here, we report the design and synthesis of oxidized bis(indolyl)methane (BIM) derivatives capable of discriminating OP simulants in pure aqueous buffered media. Comparative studies of hydroxyl and methoxy-substituted derivatives revealed distinct sensing mechanisms governed by electronic and hydrogen-bonding effects. The hydroxyl-functionalized probe (probe **1**) undergoes an initial phosphorylation step common to both diethyl cyanophosphate (DCNP) and diethyl chlorophosphate (DCP), producing an immediate colorimetric shift from orange to yellow. Critically, a subsequent time-dependent Michael addition occurs exclusively with DCNP, converting the yellow solution to colorless and enabling temporal differentiation between structurally similar OP analogues, with a limit of detection of 6.8 ± 0.3 μM (for DCNP). In contrast, the methoxy-substituted probe (probe **2**) initially engages in hydrogen-bonding interactions with both DCP and DCNP; however, Michael addition proceeds only with DCNP, generating time-dependent decrease in absorbance. Furthermore, integration of these probes onto biodegradable cellulose paper strips provides a low-cost, portable, and aqueous-compatible platform for rapid, visual detection, where distinct color transitions reflect both immediate and time-dependent chemical transformations. Overall, this study presents a sustainable, environmentally compatible sensing platform that combines mechanistic insight, high selectivity, and practical deployability for real-time monitoring of OP nerve agent mimics.

Received 7th November 2025,
Accepted 12th December 2025

DOI: 10.1039/d5an01172h

rsc.li/analyst

Introduction

Organophosphorus (OP) compounds, including both pesticides and chemical warfare agents, are highly toxic chemicals that irreversibly inhibit acetylcholinesterase, causing uncontrolled cholinergic stimulation and potentially fatal outcomes.[1] Their potency, combined with being odourless, colourless, and tasteless, underscores their recognition under the Chemical Weapons Convention (CWC) as serious threats.[2] The OP compounds covalently modify proteins, including butyrylcholinesterase and albumin, forming stable biomarkers for retrospective exposure assessment, while inducing oxidative stress and neuroinflammation linked to chronic neurological disorders.[3,4] The formation of these stable adducts and distinctive biomolecular signatures establishes OPs as valuable chemical biomarkers, making the development of sensitive and selective detection platforms essential for exposure assessment and understanding OP-induced pathophysiology.

Due to the high risk of handling authentic nerve agents, safer structural analogues (simulants) are used for detection studies. Common examples include diethyl chlorophosphate (DCP) and diisopropyl fluorophosphate (DFP) as G-type surrogates, and diethyl cyanophosphate (DCNP) as a tabun mimic.[5] While all share an electrophilic phosphoryl centre, the identity of their substituents critically influences toxicity and hydrolytic behaviour, providing a chemical basis for designing probes that selectively distinguish closely related OP simulants.[6,7] Over the years, diverse strategies, including enzyme-based assays, electrochemical platforms, surface acoustic wave devices, and optical sensors, have been explored for OP detection.[8,9] While these approaches can be highly sensitive, they often suffer from poor selectivity, cross-reactivity, and limited portability. Many optical probes incorporate nucleophilic (*e.g.*, hydroxyl, amine) or super-nucleophilic (*e.g.*, oxime, hydrazone) moieties tethered to fluorophores.[10–12] However, these probes often generate similar responses towards mul-

Department of Chemistry, BITS-Pilani Hyderabad Campus, Hyderabad-500078, India.. E-mail: nilanjandey.iisc@gmail.com, nilanjan@hyderabad.bits-pilani.ac.in

tiple OP simulants, reducing selectivity.[13,14] Recent approaches have attempted to exploit the differential reactivity of released anions such as CN^- from DCNP and Cl^- from DCP, during phosphorous-heteroatom bond hydrolysis. Yet, most of these sensors fail in fully aqueous media due to high anion hydration and competitive nucleophilic attack by water molecules, highlighting the need for water-compatible chemical reactions capable of selective discrimination.[15–17] An emerging solution lies in fine-tuning probe structures through substituent effects, where subtle modifications dramatically alter sensing pathways.[18] For instance, replacing a hydroxyl (–OH) with a methoxy (–OMe) substituent introduces distinct electronic perturbations that alter the pK_a of the indole-NH and consequently modulate its hydrogen-bond donating/accepting capacity, ultimately leading to differential interaction modes with OP simulants.

In this work, we designed and synthesised oxidised bis(indolyl)methane (BIM) based probes to achieve selective discrimination of OP simulants under aqueous buffered conditions. By systematically comparing hydroxyl and methoxy-substituted derivatives, we demonstrate how subtle structural variations at the terminal phenyl unit can alter the sensing mechanism, leading to distinct spectral responses toward different OP analogues. In particular, the hydroxyl-functionalized probe (probe **1**) undergoes an initial phosphorylation step that is common to both DCNP and DCP, but a subsequent time-delayed Michael addition is observed exclusively with DCNP. This dual-step behavior enables probe **1** to clearly differentiate DCNP from DCP, despite their structural similarity. In contrast, the methoxy analogue (probe **2**) undergoes hydrogen-bond-assisted hydrolysis followed by a single-step Michael addition. These contrasting behaviours show the synergistic role of probe design and OP leaving-group chemistry in directing the optical response (Fig. 1). Moreover, when integrated into biodegradable, cellulose filter paper strips, these probes show a clear colorimetric response, enabling rapid, on-site detection on a sustainable, low-cost, and water-compatible platform. This facile and environmentally sustainable sensing platform is suitable for safe environmental monitoring, security screening, and emergency response applications.

Design and synthesis

The oxidized bis(indolyl)methane derivatives, probes **1** and **2**, were synthesised following the procedure reported in the literature (Fig. S1 and S2).[19–21] The strategic modification of the central aryl moiety, either with a hydroxy or methoxy group, enables precise tuning of the π-conjugation length and electronic interactions within the molecule, thereby modulating both colour and optical response.[22–24] The introduction of electron-donating groups on the terminal phenyl unit can modulate the acidity of the indole NH and influence hydrogen-bonding interactions with analytes.[25]

To visualize the electronic characteristics, molecular electrostatic potential (MEP) maps were computed on the total electron density surfaces. The MEP plots shown below indicate the distribution of electron-rich (negative, red) and electron-deficient (positive, blue) regions and identify the nucleophilic and electrophilic reactive sites.[26] In both probes, the negative potential regions are mostly localised around the oxygen and nitrogen atoms, indicating possible sites of interaction *via* hydrogen bonding or electrophilic attack. As would be expected from the orbital distribution plots, the HOMO orbitals of both derivatives are concentrated over the indole π-system and the bridging methine carbon, while the LUMOs are dispersed throughout the conjugated framework in a manner that is typical for π → π* electronic transitions. In probe **2**, however, the LUMO extends more prominently across the aromatic substituent, suggesting increased conjugative stabilisation and more efficient charge re-distribution upon excitation.

For probe **1**, the HOMO and LUMO energies were calculated as −0.19683 a.u. and −0.06991 a.u., respectively, giving an

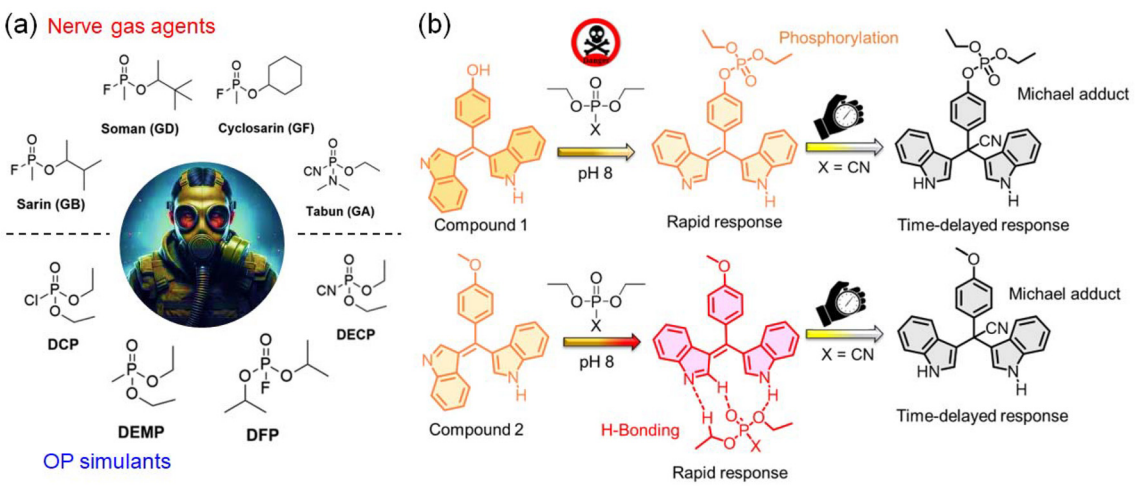

Fig. 1 (a) Chemical structures of nerve gas agents and OP simulants. (b) Proposed mechanism of detection of DCP/DCNP by probes **1** and **2** in aqueous medium (pH 8).

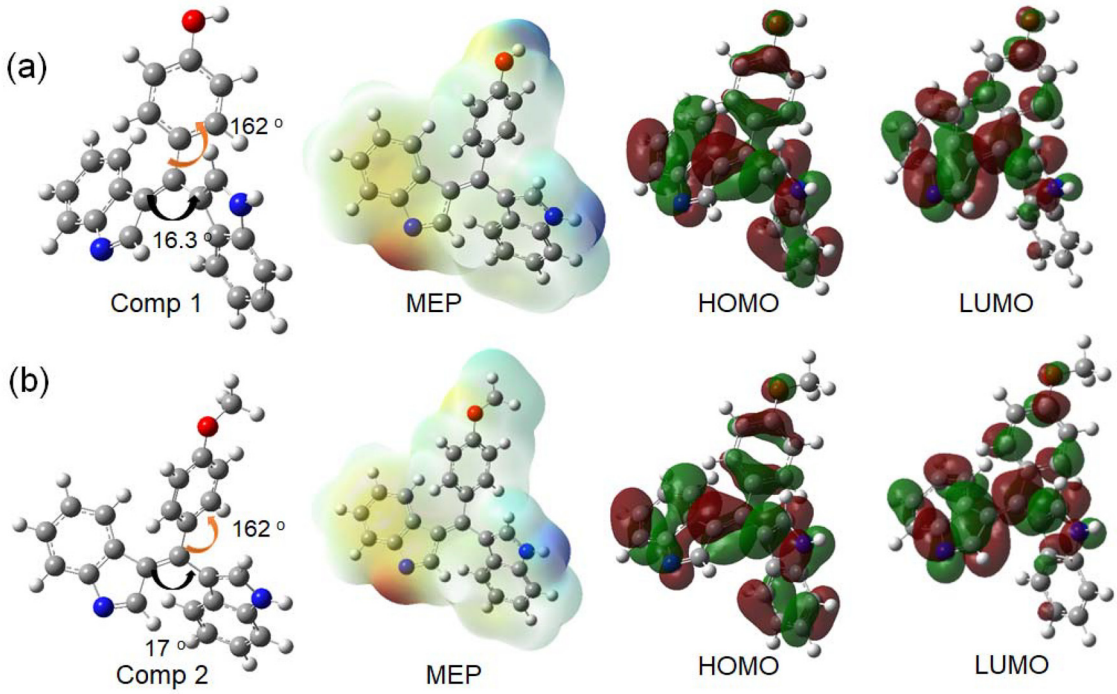

Fig. 2 Energy-optimized structures (as well as MEP) using B3LYP/6-31G* level of theory, and Frontier molecular orbital analysis of (a) compound **1** and (b) compound **2**.

energy gap (ΔE) of 0.12692 a.u. In probe **2**, the HOMO lies at −0.19544 a.u. and the LUMO at −0.06873 a.u., resulting in a slightly smaller ΔE = 0.12671 a.u. The marginally reduced HOMO–LUMO gap in probe **2** would thus point to an enhanced π-electron delocalisation and improved charge-transfer ability compared to probe **1**.[27] Geometry optimisation showed that both molecules take a slightly non-planar conformation. In probe **1**, the hydroxybenzene ring is twisted by about 162° relative to the bisindole plane, while the inter-indole dihedral angle is approximately 16.3°. Similarly, the methoxybenzene ring in probe **2** shows a comparable twist (~162°) with a slightly larger inter-indole angle (17°). Such torsional distortions are due to steric repulsion between adjacent substituents, which effectively minimises π–π stacking and contribute to the structural stability of the molecules (Fig. 2). The dipole moments of probes **1** and **2** were calculated to be 7.669 and 8.0602 D, respectively. The increased dipole moment of probe **2** directly reflects stronger intramolecular charge separation, induced by the electron-donating methoxy group. This higher dipole moment signifies greater polarisation across the conjugated backbone and correlates with its smaller HOMO–LUMO gap and greater LUMO delocalisation.

Results and discussion

Chromogenic response towards OP simulants

The detection of ionic analytes by bisindolyl-based chromogenic probes has been known in the literature. Therefore, we investigated the interaction of BIM derivative probe **1** with various organophosphate analogues in a buffered aqueous medium at pH 8.0, minimising potential pH changes due to partial hydrolysis (of analytes). Under these conditions, compound **1** displayed two partially overlapping absorption bands in the visible region with maxima near 450 nm and 505 nm. This dual-band feature arises from the presence of two closely spaced charge-transfer (CT) transitions. The hydroxyl group in compound **1** can participate in both intramolecular and solvent-assisted hydrogen bonding through the indolyl–NH and phenolic–OH sites. These interactions stabilise distinct excited states: a neutral CT state within the BIM framework and a hydrogen-bond-assisted (or partially deprotonated) CT state that is more strongly stabilised in polar protic media. The coexistence of these two CT transitions under mildly basic aqueous conditions (pH 8) accounts for the observed broad, dual-band absorption profile. Upon addition of DCNP, a rapid colour change from orange to deep yellow was observed, accompanied by a blue shift in the absorption maxima to ~480 nm and ~422 nm. Over the course of ~20 minutes, the solution gradually became colourless, with an approximately 10-fold reduction in absorbance, indicating a time-dependent reaction (Fig. 3b). Furthermore, we incubated the aqueous solution of **1** (at pH 8.0 and 25 °C) with different concentrations of DCNP for ~20 min. The UV-vis spectral analysis of these solutions suggested a dose-dependent hypochromic shift in the absorbance of **1** at 480 nm (Fig. 3a). Additionally, the detection limit for DCNP was found to be to 6.8 ± 0.3 μM. In contrast, other structurally similar nerve gas agents, such as

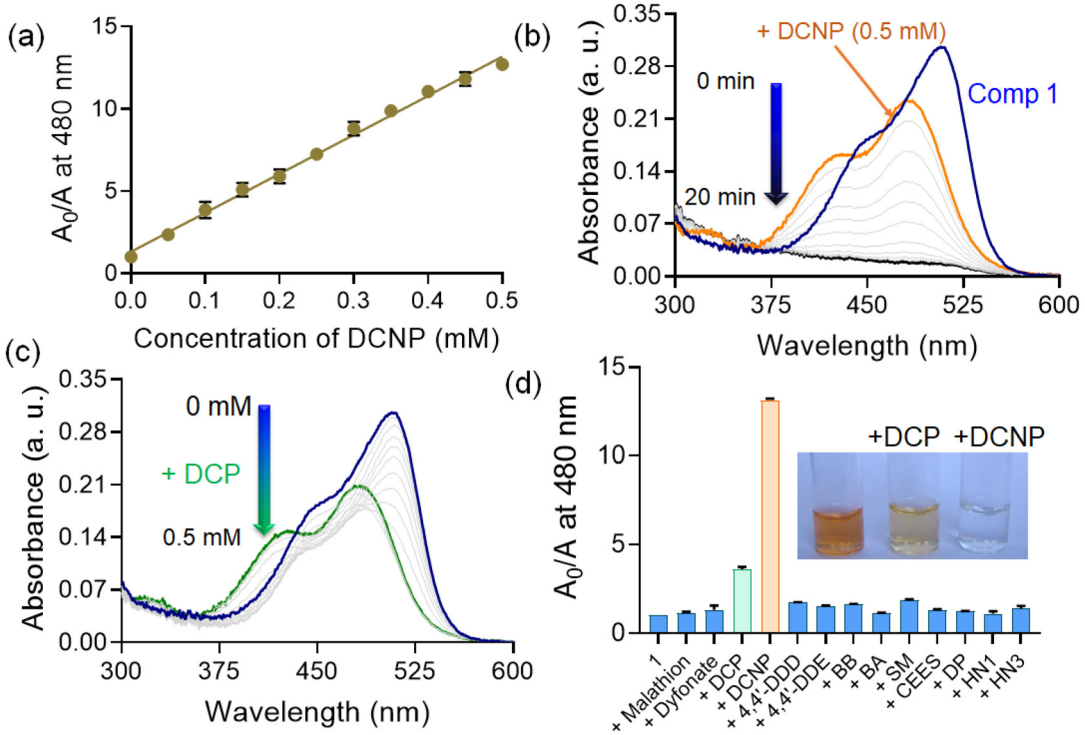

Fig. 3 (a) Point plot showing change in absorbance of compound **1** (10 μM) upon incremental addition of DCNP (0–0.5 mM) in water (pH 8) (incubation time: 30 min). (b) Time-dependent UV-visible spectra of compound **1** (10 μM) upon addition of DCNP (0.5 mM) in water (pH 8). (c) UV-visible spectra of compound **1** (10 μM) upon addition of DCP (0–0.5 mM) in water (pH 8). (d) Bar plot showing change in absorbance of compound **1** (10 μM) upon the addition of various toxic chemicals (10 equiv.) in water (pH 8).

DCP and DFP, induced only an immediate colour shift from orange to yellow, without subsequent time-dependent spectral modulation. For example, the titration of compound **1** with DCP produced blue-shifted new absorption maxima at 480 and 425 nm but lacked the subsequent time-dependent decrease in absorbance observed with DCNP (Fig. 3c). These observations suggest that the initial optical response is governed by similar recognition interactions, while the time-dependent behavior is directed by the nature of the leaving group (X = Cl for DCP, CN for DCNP), which directs the subsequent chemical transformations.[28,29] Furthermore, the UV-visible spectra of the probe were recorded in the presence of a wide range of toxic chemicals and warfare agents (10 equiv.), such as malathion, dyfonate, benzyl bromide *etc.* (Fig. S3). These analytes elicited no spectral response, highlighting the probe's selectivity towards DCNP (Fig. 3d). Additionally, the stability of compound **1** in pH 8 buffer was evaluated by monitoring its absorbance over 16 days. The results show negligible changes in absorbance or colour intensity, indicating excellent photochemical and structural stability under these conditions (Fig. S4).

To evaluate the DCNP-induced time-dependent spectral changes, we conducted kinetics experiments at temperatures ranging from 25 °C to 55 °C in the presence of excess DCNP (Fig. 4). The reactions followed pseudo-first-order kinetics, with the rate of color fading increasing at higher temperatures (7.0×10^{-2} to 47.3×10^{-2} min^{-1}). Thermodynamic parameters derived from Arrhenius and Eyring–Polanyi analyses revealed a positive $\Delta H^{\#}$ (~11 kcal mol^{-1}), indicative of an exothermic interaction, and a negative $\Delta S^{\#}$ (~−25 cal mol^{-1} K^{-1}), suggesting an associative mechanism.[28]

The pH dependence of the **1**. DCNP interaction was further investigated by performing the reaction in buffered solutions across a range of pH values. The cyanide-mediated time-dependent step proceeded significantly more slowly at pH 7, likely due to the reduced availability of free cyanide ions (pK_a of HCN = 9.3), whereas under alkaline conditions the reaction occurred rapidly, consistent with the self-hydrolysis of the phosphoester (Fig. 5a).[30] To ensure that the observed spectral changes were intrinsic to the probe-analyte interaction, we tested the reaction in different buffer systems (Tris-HCl, HEPES, PBS, and phosphate) at pH 8.0. In all cases, we observed comparable responses, confirming that the buffer components exerted minimal interference on the time-dependent CN-mediated reaction (Fig. 5b).

Mechanistic insights into probe-OP analogue interactions

To investigate the mode of interaction between probe **1** and OP analogues, we performed a series of spectroscopic experiments. We analysed the Job's plot, which revealed a 1 : 1 interaction stoichiometry for both DCNP and DCP (Fig. 5c and d). Furthermore, we analysed the mass spectra of probe **1**. DCP,

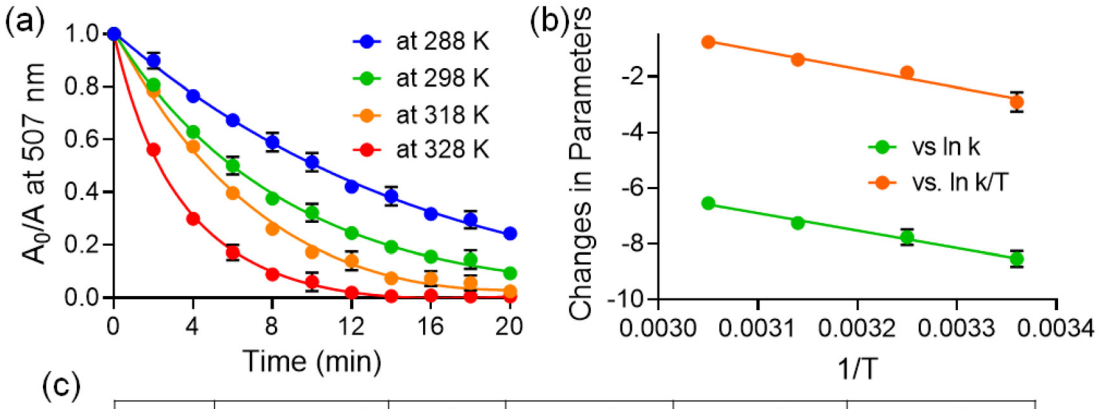

(c)

Temp (°C)	Rate (min^{-1})	r^2	$\Delta G^{\#}$ ($kcal.mol^{-1}$)	$\Delta H^{\#}$ ($kcal.mol^{-1}$)	$\Delta S^{\#}$ ($kcal.mol^{-1}$)
25	7.0×10^{-2}	0.9975	18.98	11.41	-25.42
35	15.9×10^{-2}	0.9984	19.23	11.39	-25.48
45	24.8×10^{-2}	0.9986	19.49	11.37	-25.55
55	47.3×10^{-2}	0.9919	19.74	11.35	-25.61

Fig. 4 (a) Arrhenius plot depicting the temperature dependence of the rate constants for the interaction between DCNP and compound **1**. (b) Eyring–Polanyi plot of ln (*k*/*T*) *versus* 1/*T*, used to determine the activation parameters-activation free energy ($\Delta G^{\#}$), activation enthalpy ($\Delta H^{\#}$), and activation entropy ($\Delta S^{\#}$) for the interaction of DCNP with **1**. (c) Summary table of the calculated kinetic and thermodynamic parameters associated with the interaction between DCNP and **1**.

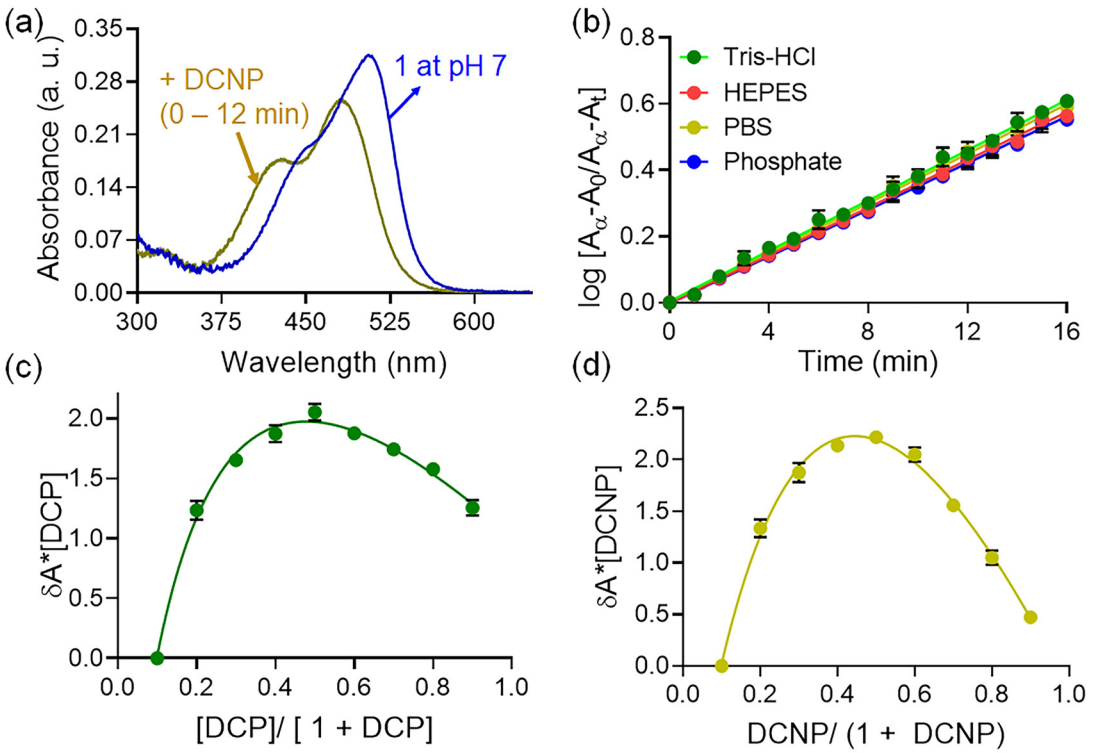

Fig. 5 (a) Time-dependent UV-Visible spectra of compound **1** (10 μM) upon addition of DCNP (0.5 mM) in water (pH 7). (b) Time-dependent change in absorbance of compound **1** (10 μM) upon addition of DCP (0.5 mM) in different pH-buffered medium. (c) Job's plot of compound **1** with DCP. (d) Job's plot of compound **1** with DCNP.

which showed a new peak at m/z 473.04, corresponding to the phosphorylated adduct, confirming that the initial interaction involves phosphorylation of compound **1** (Fig. 6a).[31] This first step of phosphorylation was found to be common for both DCP and DCNP. To elucidate the nature of the interaction between probe **1** and DCP, comparative FTIR spectra for the individual components (probe **1** and DCP) and for their reaction mixture (**1** + DCP adduct) were analysed (Fig. 6b).

The spectrum of pure probe **1** (green trace) exhibits characteristic absorption bands at ~3390 cm^{-1} (N–H stretching), 1602 cm^{-1} (aromatic C=C/C=N stretching), and 1250–1270 cm^{-1} (C–N and C–O vibrations).[32] The FTIR spectrum of DCP (blue trace) shows prominent bands at 1283 cm^{-1}, assigned to P=O stretching, and 1026 cm^{-1}, corresponding to P–O–C(alkyl) stretching vibrations.[33] Upon reaction between probe **1** and DCP, the resulting adduct (red trace) displays distinct spectral changes indicative of chemical transformation. Two new, intense bands emerge at ~1023 cm^{-1} and in the 1180–1320 cm^{-1} region. These can be assigned to P–O–C(alkyl) and overlapping P=O/P–O–C(aryl) stretching modes, respectively, confirming the incorporation of a phosphoryl moiety into the probe framework, while the IR bands of the indole framework remain largely unchanged. To distinguish a chemical reaction from a physical mixture, a control FTIR spectrum was recorded for an equimolar, unreacted mixture of probe **1** and DCP prepared under identical conditions (without allowing sufficient reaction time). In this case, no new absorption bands appeared, and only a simple superposition of the individual component spectra was observed. This confirms that the new features in the **1** + DCP adduct spectrum arise from true covalent phosphorylation rather than noncovalent or physical interactions. Collectively, these FTIR observations provide direct spectroscopic evidence supporting phosphorylation of the –OH moiety of probe **1**.

Interestingly, divergence in the reaction pathway was observed in the subsequent time-dependent step. Upon exposure to DCNP, probe **1** exhibited a gradual decrease in absorbance over ~20 min, whereas no significant changes were observed with DCP. To investigate this further, we examined the interaction of probe **1** with potassium cyanide (KCN) under similar conditions (Fig. 6c). In the presence of KCN, a similar time-dependent decrease in absorbance was observed; however, the process occurred much faster (~10 min) and lacked the initial blue shift, characteristic of phosphoester products. In contrast, the reaction with DCNP was slower (~20 min), consistent with the gradual, stepwise release of cyanide ions during its hydrolysis (Fig. S5).[28] These results demonstrate that the differences in kinetics and observed spectral responses arise directly from the instantaneous availability of cyanide with KCN versus the stepwise generation of cyanide from DCNP.[34]

To further substantiate the critical involvement of cyanide ions released from DCNP in governing the optical response of probe **1**, a series of control experiments employing Cu^{2+} ions was conducted. When Cu^{2+} was introduced into the solution of probe **1** prior to the addition of DCNP, no time-dependent change in absorbance of the probe was observed. This finding indicates that Cu^{2+} effectively sequesters any cyanide liberated from DCNP, thereby inhibiting nucleophilic attack (Michael addition). Similarly, when Cu^{2+} was added to probe **1**. DCNP

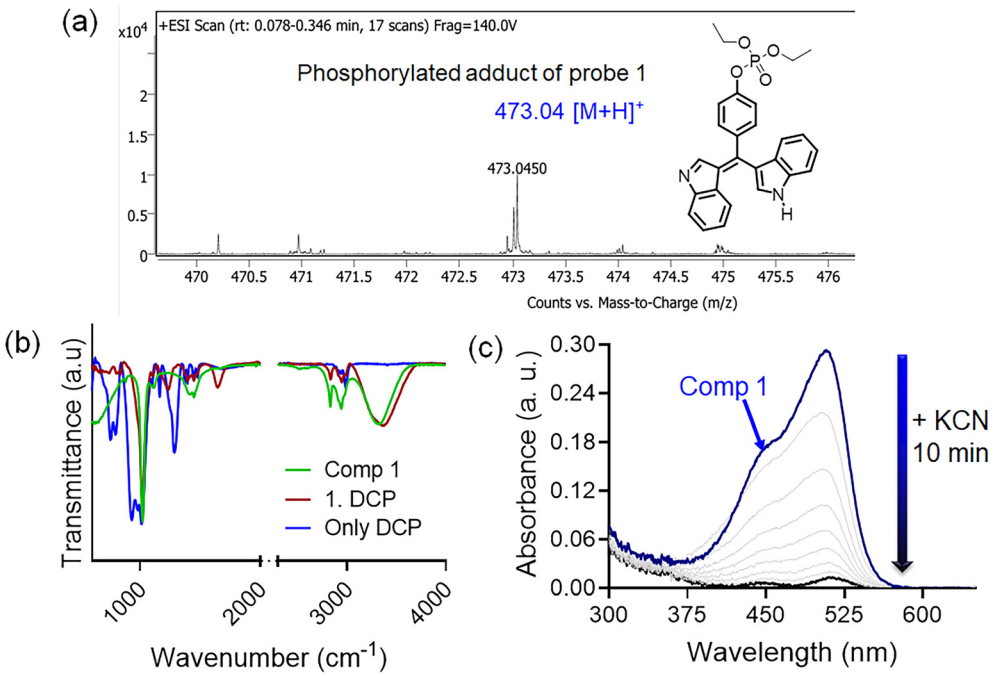

Fig. 6 (a) Mass spectra of **1**. DCP. (b) FTIR spectra of **1**. DCP. (c) Time-dependent UV-Visible spectra of probe **1** upon addition of KCN in water (pH 8).

mixture (immediately), the reaction progression was suppressed, as evidenced by the absence of spectral changes. This can be attributed to the preferential coordination of free cyanide by Cu^{2+} ions. In contrast, when Cu^{2+} was introduced to probe **1**. DCNP mixture (after the reaction had reached completion *i.e.*, after 20 minutes), no additional spectral changes were observed, and the quenched absorbance spectra persisted. This finding indicates that the released cyanide (from DCNP) is completely consumed or tightly bound during the reaction period. Overall, these results provide clear mechanistic evidence that the decrease in absorbance of probe **1** is directly governed by *in situ*-generated cyanide ions, which act as the reactive nucleophile (Fig. 7a).

To further explore selectivity, we tested compound **1** against other competitive anionic species, including S^{2-}, N_3^-, H_2PO^{4-}, and AcO^- at pH 8.0. A distinct color change from orange to colorless occurred specifically in the presence of cyanide, but the initial color change from orange to yellow observed with DCNP was absent. This provided a clear optical distinction between free cyanide and phosphoester analytes and confirmed that exogenously added cyanide does not interfere with the DCNP interaction, further supporting the phosphoester hydrolysis of DCNP.

Nevertheless, to validate the structural basis of this process, we compared the behavior of oxidized compound **1** with its unoxidized precursor (Fig. 7b). Upon addition of DCP/DCNP (in pH 8), the precursor displayed red-shifted absorption bands attributable to phosphorylation, but no subsequent time-dependent decrease in absorbance was observed, highlighting the requirement of the electron-deficient double bond for Michael addition in oxidized compound **1**. Furthermore, we performed ^{1}H-NMR titration of compound **1** in a DMSO-d_6/D_2O (1 : 1) mixture after ~30 min incubation with DCP/DCNP (Fig. 7c). A small amount of NaOH was added to maintain the solution under basic conditions, promoting cyanide release and enabling clear spectral observation. The ^{1}H-NMR spectra of **1**. DCP showed upfield shifts and broadening of aromatic peaks, with the maximum changes observed at the indolyl sites. In contrast, the addition of DCNP induced a pronounced upfield shift in the ^{1}H-NMR signals of compound **1** along with the appearance of new peaks. The upfield shifts indicated accumulation of negative charge during the interaction, while the new peaks suggested formation of covalent species. We propose that these new peaks correspond to a Michael-type nucleophilic addition of cyanide (released during DCNP hydrolysis), to the electron-deficient double bond of the oxidised BIM scaffold. This reaction produces a chemodosimetric adduct, in which the chemical environments of the indole moieties are distinctly altered. Similarly, ^{13}C-NMR of probe **1** in the presence of DCNP displayed the formation of a new peak at 49.1 ppm owing to the generation of a quaternary carbon centre (Fig. S6). We further confirmed this transform-

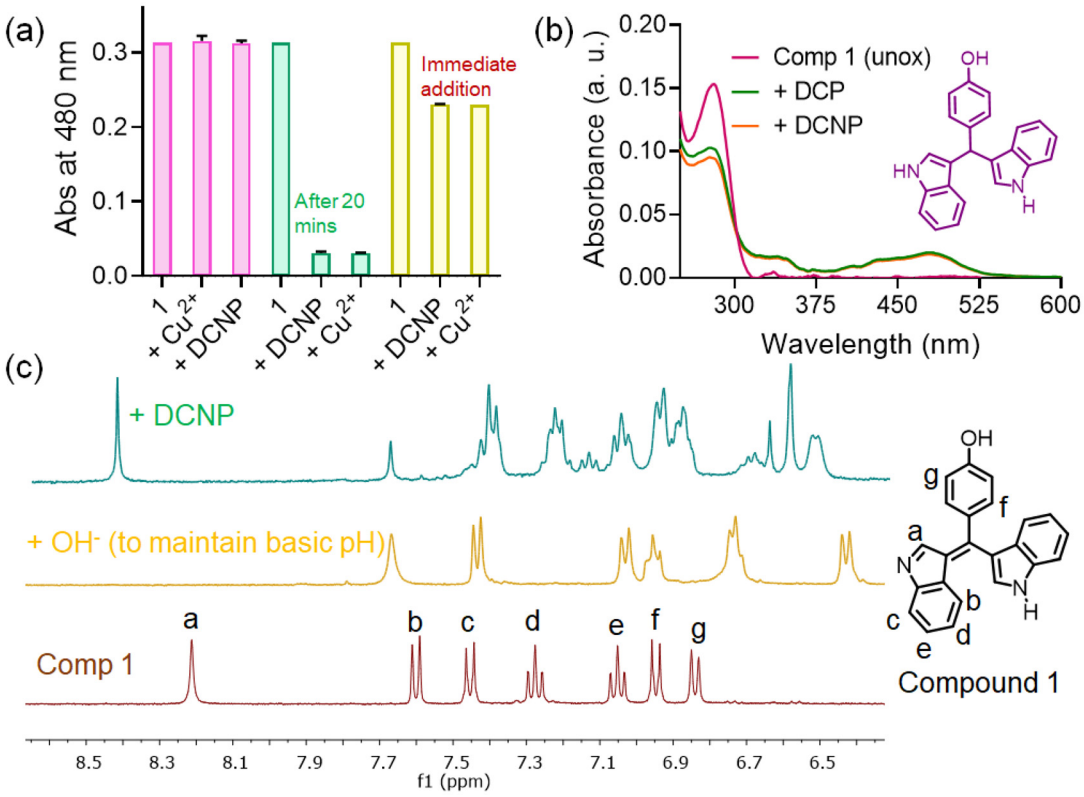

Fig. 7 (a) Bar plot showing change in absorbance (at 480 nm) of probe **1** (10 μM) upon addition of Cu^{2+} ions and DCNP in water (pH 8). (b) UV-Visible spectra of unoxidized probe **1** (10 μM) upon the addition of DCP/DCNP in water (pH 8). (c) Partial ^{1}H-NMR of the probe **1** in the presence of DCNP in DMSO-d_6/D_2O (1 : 1) mixture (incubation time: 30 min).

ation by mass spectrometry, which showed a new peak at m/z 499, corresponding to the 1 : 1 Michael adduct (Fig. S7). The FTIR spectrum of the adduct (1 + DCNP, after 30 minutes) shows distinct bands at 1023 cm^{-1} (P–O–C(alkyl)) and within 1346–1487 cm^{-1} (P═O/P–O–C(aryl)), confirming the covalent linkage of the phosphate group. The characteristic nitrile (C≡N) band, which is sharp at 2196 cm^{-1} in free DCNP, becomes broad and slightly red-shifted (~2243 cm^{-1}) in the adduct, reflecting electronic perturbation of the cyanide moiety due to conjugation with the indolyl system (Fig. S8). Taken together, these results establish a dual-step mechanism: an initial phosphorylation step common to both DCP and DCNP, followed by a unique cyanide-mediated Michael addition that occurs exclusively with DCNP.

To explore the nature of the terminal substituent in sensing, we examined probe **2**, which bears a methoxy substituent attached to the phenyl ring. Unlike probe **1**, compound **2** exhibited a single, blue-shifted absorption band centred near 430 nm. The methoxy substituent donates electron density to the π-system through resonance but cannot form strong hydrogen bonds. As a result, its excited state experiences only limited solvent stabilisation, giving rise to one dominant intramolecular CT transition (Fig. 8a). The spectral differences between compounds **1** and **2** therefore reflect substituent-dependent modulation of CT processes and hydrogen-bonding effects, consistent with prior reports on oxidized *p*-substituted di(indolyl)arylmethanes.[19]

Upon addition of DCP in buffered solution at pH 8.0, a distinct red shift of the absorption band was observed (from 425 to 485 nm), whereas addition of DCNP resulted in a gradual decrease in absorbance without a significant shift in absorption maxima (Fig. 8b). These observations contrast with probe **1**, where the hydroxyl substituent enabled direct phosphorylation, leading to a distinct spectral response. The difference in the absorbance response could be attributed to the role of the terminal substituents. In probe **2**, the methoxy group is unable to undergo phosphorylation, and the initial interaction of both DCP and DCNP occurs primarily through hydrogen bonding between the phosphoryl oxygen atoms and the indolyl–NH group. In the case of DCP, this hydrogen-bonding interaction alone accounts for the observed red shift in absorption, with no subsequent covalent modification. In contrast, with DCNP, the initial hydrogen-bonding facilitates a secondary reaction, where the cyanide released during hydrolysis attacks the electron-deficient meso carbon of the BIM scaffold of probe **2**. This Michael addition pathway leads to a decrease in absorbance, representing the time-delayed response characteristic of DCNP.

The interaction between compound **2** and DCP was further examined by FTIR spectroscopy to validate the proposed triple

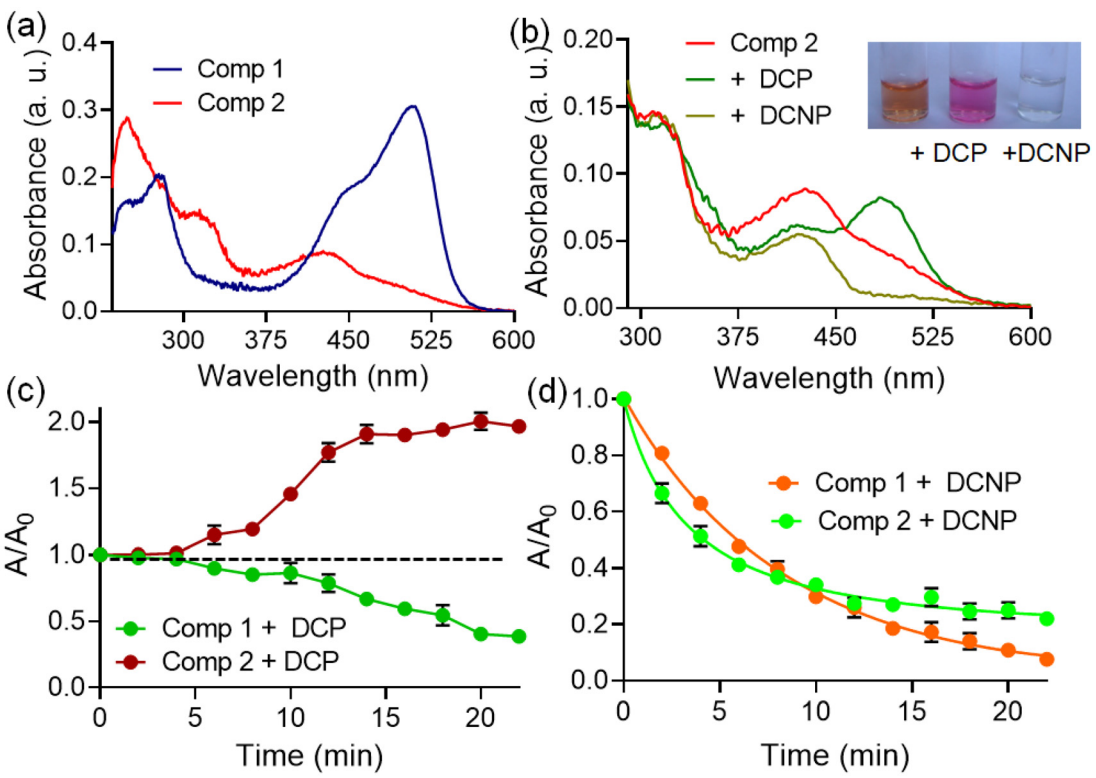

Fig. 8 (a) UV-Visible spectra of probe **1** and probe **2** (10 μM) in water (pH 8). (b) UV-Visible spectra of probe **2** (10 μM) upon the addition of DCP/DCNP (0.5 mM) in water (pH 8). (c) Point plot showing time-dependent change in absorbance of probe **1** and **2** (10 μM) upon addition of DCP (0.5 mM) in water (pH 8). (d) Point plot showing time-dependent change in absorbance of probe **1** and **2** (10 μM) upon addition of DCNP (0.5 mM) in water (pH 8).

hydrogen-bonding interaction. In the **2**. DCP adduct, the P═O band (of DCP) becomes broadened and red-shifted to ~1265 cm^{-1}, reflecting electronic perturbation of the phosphoryl group due to hydrogen-bonding. Significantly, the N–H stretching vibration of the indolyl fragment (~3343 cm^{-1}) shifts to a lower wavenumber (~3264 cm^{-1}) with pronounced broadening, confirming its participation in H-bonding with the phosphoryl oxygen. A second, weaker C–H···O═P hydrogen bond is evidenced by the downshift and broadening of the aromatic C–H stretching region (~2906 cm^{-1}) (Fig. S9a).

In contrast, upon addition of DCNP to comp **2**, the FTIR spectrum of the adduct shows three key changes: (i) a nitrile band persists in the ~2167 cm^{-1} region but becomes noticeably broader than in free DCNP, indicating modified C≡N environment; (ii) new, intense phosphate bands appear at ~1034 cm^{-1} and within the 1030–1200 cm^{-1} region, consistent with the P–O–C(alkyl) and overlapping P═O/P–O–C(aryl) stretches of an aryl phosphate ester; and (iii) the indole and aromatic bands of the scaffold remain essentially unchanged, indicating that the core structure of **2** is retained (Fig. S9b). Additionally, the LC-MS spectrum of the reaction mixture exhibits a new molecular ion peak at *m*/*z* 377.9, consistent with the formation of a proposed adduct (Fig. S10).

Moreover, substitution at the terminal position also influenced the protonation pK_a of the indolyl units. The probe **1** (hydroxy-substituted) exhibits two pK_a values (4.3 for phenolic–OH and 7.9 for indolyl–NH) corresponding to its two distinct acidic sites, while probe **2** (methoxy-substituted) is characterised by a single, relatively low pK_a (6.4) due to the presence of only one acidic NH group. The higher pK_a of the indolyl NH in probe **2**, compared to probe **1**, indicates that the indolyl groups in probe **2** are more basic, consistent with the electron-donating effect of the methoxy group. Furthermore, we systematically assessed the response kinetics of our probes toward DCNP, observing that probe **2** demonstrates a significantly faster reaction compared to probe **1** (Fig. 8c and d).

The optimized geometry and MEP map of probe **1**. DCNP complex reveals distinct charge separation upon anion coordination (Fig. S11). The MEP distribution reveals a concentrated region of negative potential (red) localised over the hydroxyl oxygen and the coordinated cyanide moiety, denoting areas of high electron density. In contrast, the indole and methine units exhibit regions of moderate positive potential (blue–green), indicative of polarisation effects induced by the anionic coordination. Conformational analysis of the optimised geometry demonstrates a substantial loss of planarity upon DCNP binding, as reflected by a decrease in the dihedral angle between the indole subunits to 7.22° and a torsional angle of 114° between the indole system and the hydroxybenzene moiety. This deviation from the near-coplanar configuration of the free probe is attributed to electronic and steric perturbations induced by the coordinated DCNP anion, which initially enhances core planarity but overall disrupts the conjugated π-network and alters the electron density distribution. The electronic reorganization is further corroborated by frontier orbital and dipole moment analysis. The HOMO and LUMO energies of the DCNP adduct are −0.20618 a.u. and −0.01255 a.u., respectively, resulting in a widened energy gap of 0.19363 a.u. compared to the free probe. The dipole moment of the adduct is calculated to be 6.3942 D, reflecting a decrease in overall charge separation and supporting the observed loss of planarity and disruption of the π-conjugated network.

Portable paper strips for OP simulant discrimination

In real-world scenarios, trace amounts of organophosphorus compounds can be found in diverse environmental matrices. For example, DCP has been detected in aqueous environments, while DCNP persists in soil and water, highlighting their contamination potential and the need for sensitive detection. Given their acute toxicity (LD50 ~1.4 mg kg^{-1} for DCNP and ~11 mg kg^{-1} for DCP), early identification at low micromolar concentrations (~1–10 μM) is essential for safety and remediation.[35]

In this context, probe **1** was employed as a molecular sensor due to its high responsiveness, aqueous compatibility, and facile integration into practical platforms. To develop a portable sensing platform, identically-sized Whatman-41 filter papers were immersed in a 2 mM solution of probe **1** in DMSO, allowed to absorb the probe, and then dried at 60 °C to produce uniform coated strips. The FTIR spectra of the probe-coated paper confirmed the successful immobilization of the probe on the paper by revealing characteristic probe IR bands distinct from the paper substrate (cellulose) (Fig. 9a). The stability of the probe-coated strips was further validated by monitoring absorbance over 15 days, demonstrating excellent sensor durability (Fig. 9b). Additionally, the FESEM images confirmed that the microstructure and structural integrity of the paper remained intact after probe coating, indicating that the immobilization process did not alter or damage the paper substrate (Fig. 9d inset). This observation supports the suitability of the filter paper as a stable platform for probe integration, ensuring consistent sensor performance without compromising the mechanical or physical properties of the substrate. To assess real-world applicability, the performance of the strips was systematically evaluated under varying environmental conditions. The strips retained consistent absorbance and sensing efficiency across a temperature range of 10–50 °C, under relative humidity levels from 20% to 90%, and in buffered solutions with pH ranging from 5 to 9. These tests revealed negligible effects of temperature, humidity, or pH on the stability of the immobilised probe and its sensing response, thereby underscoring the robustness and reliability of the platform for diverse field conditions.

Upon exposure to DCP and DCNP, the precoated strips exhibited an immediate and visible color change from orange to yellow, enabling naked-eye detection. Notably, only DCNP-induced colouration gradually faded to colourless over 25 minutes, providing temporal discrimination between analytes (Fig. 9c). The changes in color intensity were quantified using readily available image processing software ImageJ (Fig. 9d). This low-cost, biodegradable, and disposable paper-

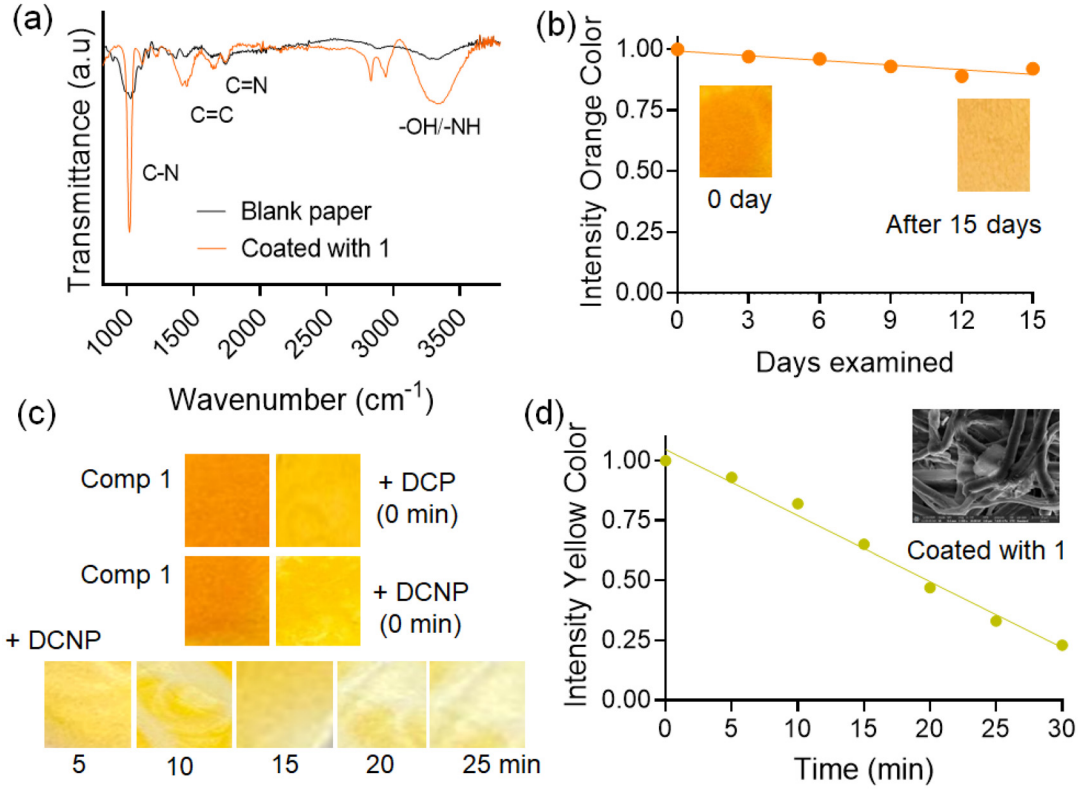

Fig. 9 (a) FTIR spectra of the probe **1**-coated and uncoated paper strip. (b) Changes in colour intensity of pre-coated paper over 15 days, quantified by ImageJ software. (c) Change in colour of paper strips coated with **1** upon addition of DCP/DCNP at 0 min; and DCNP over 25 minutes under daylight. (d) Time-dependent change in colour intensity of pre-coated paper upon addition of DCNP (0.5 mM), quantified by ImageJ software. Inset: FESEM image of pre-coated paper.

strip sensor provides a rapid, user-friendly platform for real-time environmental monitoring of organophosphorus nerve agent mimics.[36–39] Its sustainability, ease of fabrication, and eco-compatible nature highlight its promise for widespread application in environmental surveillance, safety assessments, and defence monitoring.[40]

Conclusion

In summary, we have demonstrated that oxidised bis(indolyl) methane (BIM) probes can selectively discriminate hazardous organophosphorus (OP) simulants in aqueous media through a dual-step recognition mechanism. The hydroxyl-substituted probe **1** undergoes an initial phosphorylation with both DCNP and DCP, generating a rapid orange-to-yellow color change, followed by a cyanide-mediated Michael addition exclusive to DCNP, converting the solution to colorless. The methoxy-substituted probe **2** interacts with DCP/DCNP primarily *via* hydrogen bonding, with the Michael addition occurring selectively with DCNP. These results highlight the critical role of electronic effects and leaving-group chemistry in directing selective optical responses. Nevertheless, immobilisation of the probes on biodegradable cellulose strips enables rapid, visible color changes, allowing straightforward, on-site discrimination of OP simulants without the need for specialised instruments or technical training. The platform is highly robust across varying pH, temperature, and humidity conditions. This sustainable, water-compatible, and portable sensor provides a practical tool for chemical-warfare agent detection, hazard assessment, emergency response, and environmental monitoring.

Conflicts of interest

There are no conflicts to declare.

Data availability

Data will be available from authors on reasonable request.

Supplementary information (SI) is available. See DOI: https://doi.org/10.1039/d5an01172h.

Acknowledgements

N. D. thanks BITS-Pilani (Hyderabad campus) for all technical and financial support. R. S. F. thanks BITS Pilani (Hyderabad) for a research fellowship. The authors also thank the central

analytical facilities of BITS-Pilani for providing technical support and laboratory facilities. The authors also gratefully acknowledge the Ministry of Education (MoE), Government of India, for financial support under the STARS scheme (MoE-STARS/STARS-2/2023-0300).

References

1 T. C. Marrs, Toxicology of organophosphate nerve agents, *J. Chem. Works Treat.*, 2007, **191**, 191–221.
2 V. Aroniadou-Anderjaska, T. H. Figueiredo, M. de Araujo Furtado, V. I. Pidoplichko and M. F. Braga, Mechanisms of organophosphate toxicity and the role of acetylcholinesterase inhibition, *Toxics*, 2023, **11**(10), 866.
3 J. Wang, F. Sun, X. Lu, R. Gao, C. Pei and H. Wang, Retrospective detection for V-type OPNAs exposure via phosphonylation and disulfide adducts in albumin, *Sci. Rep.*, 2022, **12**(1), 10979.
4 J. Marsillach, L. G. Costa and C. E. Furlong, Protein adducts as biomarkers of exposure to organophosphorus compounds, *Toxicology*, 2013, **307**, 46–54.
5 Q. Chen, J. Liu, S. Liu, J. Zhang, L. He, R. Liu and K. Zhang, Visual and rapid detection of nerve agent mimics in gas and solution phase by a simple fluorescent probe, *Anal. Chem.*, 2023, **95**(9), 4390–4394.
6 N. Dey, J. Kulhanek, F. Bures and S. Bhattacharya, Imidazole-functionalized Y-shaped push–pull dye for nerve agent sensing as well as a catalyst for their detoxification, *J. Org. Chem.*, 2021, **86**(21), 14663–14671.
7 S. Mondal and N. Dey, Comparative analysis of monomeric vs. dimeric salen fluorescent probes: transition from a turn-on to ratiometric response towards nerve gas agents in organic to aqueous media, *Mater. Adv.*, 2025, **6**(3), 977–991.
8 Y. Yang, H. F. Ji and T. Thundat, Nerve agents detection using a Cu^{2+}/L-cysteine bilayer-coated microcantilever, *J. Am. Chem. Soc.*, 2003, **125**(5), 1124–1125.
9 A. J. Russell, J. A. Berberich, G. F. Drevon and R. R. Koepsel, Biomaterials for mediation of chemical and biological warfare agents, *Annu. Rev. Biomed. Eng.*, 2003, **5**(1), 1–27.
10 S. Royo, R. Martínez-Máñez, F. Sancenón, A. M. Costero, M. Parra and S. Gil, Chromogenic and fluorogenic reagents for chemical warfare nerve agents' detection, *Chem. Commun.*, 2007, **46**, 4839–4847.
11 T. J. Dale and J. Rebek Jr., Hydroxy oximes as organophosphorus nerve agent sensors, *Angew. Chem.*, 2009, **121**(42), 7990–7992.
12 S. Han, Z. Xue, Z. Wang and T. B. Wen, Visual and fluorogenic detection of a nerve agent simulant via a Lossen rearrangement of rhodamine-hydroxamate, *Chem. Commun.*, 2010, **46**(44), 8413–8415.
13 D. Knapton, M. Burnworth, S. J. Rowan and C. Weder, Fluorescent organometallic sensors for the detection of chemical-warfare-agent mimics, *Angew. Chem., Int. Ed.*, 2006, **45**(35), 5825–5829.
14 Z. Lei and Y. Yang, A concise colorimetric and fluorimetric probe for sarin related threats designed via the "covalent-assembly" approach, *J. Am. Chem. Soc.*, 2014, **136**(18), 6594–6597.
15 A. M. Costero, M. Parra, S. Gil, R. Gotor, R. Martínez-Mañez, F. Sancenón and S. Royo, Selective detection of nerve agent simulants by using triarylmethanol-based chromogenic chemodosimeters, *Eur. J. Org. Chem.*, 2012, **2012**(26), 4937–4946.
16 Y. Liu and M. Bonizzoni, A supramolecular sensing array for qualitative and quantitative analysis of organophosphates in water, *J. Am. Chem. Soc.*, 2014, **136**(40), 14223–14229.
17 A. K. Das, S. Goswami, C. K. Quah and H. K. Fun, Relay recognition of F^- and a nerve-agent mimic diethyl cyanophosphonate in mixed aqueous media: discrimination of diethyl cyanophosphonate and diethyl chlorophosphate by cyclization induced fluorescence enhancement, *RSC Adv.*, 2016, **6**(22), 18711–18717.
18 Y. Jung and D. Kim, A selective fluorescence turn-on probe for the detection of DCNP (nerve agent tabun simulant), *Materials*, 2019, **12**(18), 2943.
19 B. Chettri, S. Jha and N. Dey, Tuning anion binding properties of bis(indolyl)methane receptors: effect of substitutions on optical responses, *Spectrochim. Acta A*, 2023, **287**, 121979.
20 R. S. Fernandes and N. Dey, Modulation of analytical performance of a bifunctional optical probe at the micelle-water interface: selective sensing of histidine in biological fluid, *Asian J. Org. Chem.*, 2022, **11**(8), e202200257.
21 H. V. Barkale and N. Dey, Membrane-bound bisindolyl-based chromogenic probes: analysis of cyanogenic glycosides in agricultural crops for possible remediation, *ACS Appl. Bio Mater.*, 2024, **8**(1), 189–198.
22 R. S. Fernandes and N. Dey, Tuning fluorescence properties of BIM probes via clay integration: targeting rifampicin with improved selectivity, *Chem. – Asian J.*, 2025, **20**(6), e202401354.
23 R. S. Fernandes, A. Gangopadhyay and N. Dey, Shedding light on protein aggregates by bisindolyl-based fluorogenic probes: unveiling mechanistic pathways and real-time tracking of protein aggregation, *Biomacromolecules*, 2025, **26**(3), 1461–1475.
24 R. S. Fernandes and N. Dey, Bioinspired composite materials with amplified clusteroluminescence: chemodosimetric interaction targeting hypochlorite in aqueous medium, *ACS Mater. Au*, 2024, **5**(2), 308–319.
25 R. S. Fernandes and N. Dey, Exploring the synergistic effect of aggregation and hydrogen bonding: a fluorescent probe for dual sensing of phytic acid and uric acid, *J. Mater. Chem. B*, 2024, **12**(45), 11789–11799.
26 S. Pise and N. Dey, Modulation in the charge transfer characteristics of flexible bis-benzimidazole probes: independent sensing mechanisms for Hg^{2+} and F^-, *Dalton Trans.*, 2025, **54**(7), 2896–2907.

27 J. Kumar, N. Kumar and P. K. Hota, Optical properties of 3-substituted indoles, *RSC Adv.*, 2020, **10**(47), 28213–28224.
28 N. Dey, S. Jha and S. Bhattacharya, Visual detection of a nerve agent simulant using chemically modified paper strips and dye-assembled inorganic nanocomposite, *Analyst*, 2018, **143**(2), 528–535.
29 S. Mondal, B. Krishna, S. Roy and N. Dey, Discerning toxic nerve gas agents via a distinguishable "turn-on" fluorescence response: multi-stimuli responsive quinoline derivatives in action, *J. Anal. Appl. Chem.*, 2024, **149**(11), 3097–3107.
30 R. S. Fernandes, J. Kumari, A. Gangopadhyay, D. Sriram and N. Dey, Tailoring bisindolyl methane derivatives for dual applications: substituent-directed probing of cyanide ions and anti-tubercular activity, *J. Mol. Liq.*, 2024, **410**, 125266.
31 B. Sen, M. Rabha, S. K. Sheet, D. Koner, N. Saha and S. Khatua, Bis-heteroleptic Ru(II) polypyridine complex-based luminescent probes for nerve agent simulant and organophosphate pesticide, *Inorg. Chem. Front.*, 2021, **8**(3), 669–683.
32 R. J. Reshi and G. P. L. M. Malar, Spectroscopic studies and molecular docking investigation of bisindolyl methane interaction with casein nanoparticles, *J. Mol. Struct.*, 2025, **1348**, 143230.
33 G. Keglevich, R. E. Puskás, A. Grün, I. Csontos and I. Greiner, Monitoring the phosphorylation of phenol derivatives with diethyl chlorophosphate in liquid-liquid and solid-liquid phase by in situ Fourier transform infrared spectroscopy, part II, *Phosphorus, Sulfur Silicon Relat. Elem.*, 2010, **185**(11), 2333–2340.
34 N. Kumari, S. Jha and S. Bhattacharya, A chemodosimetric probe based on a conjugated oxidized bis-indolyl system for selective naked-eye sensing of cyanide ions in water, *Chem. – Asian J.*, 2012, **7**(12), 2805–2812.
35 H. S. Sarkar, A. Ghosh, S. Das, P. K. Maiti, S. Maitra, S. Mandal and P. Sahoo, Visualisation of DCP, a nerve agent mimic, in catfish brain by a simple chemosensor, *Sci. Rep.*, 2018, **8**(1), 3402.
36 R. S. Fernandes, S. Ch, B. Ghosh and N. Dey, Sulfide-induced concentration-dependent distinct optical response: unique chromogenic probe developed for analyzing fecal contamination in water and intracellular imaging applications, *ACS Sustainable Chem. Eng.*, 2024, **12**(12), 4922–4932.
37 R. S. Fernandes and N. Dey, Oxidized bis(indolyl)methane derivatives with diverse signaling units: an excitation-dependent fluorescence response toward heavy metal pollutants in an aqueous medium, *Ind. Eng. Chem. Res.*, 2023, **62**(50), 21536–21545.
38 A. Pal and N. Dey, A chromogenic anthraimidazoldione probe for ratiometric analysis of Hg2+ exclusively at mesoscopic interface: Screening of real-life biological samples, *Colloids Surf. A: Physicochem. Eng. Asp.*, 2024, **687**, 133397.
39 X. Zhou, Y. Zeng, C. Liyan, X. Wu and J. Yoon, A fluorescent sensor for dual-channel discrimination between phosgene and a nerve-gas mimic, *Angew. Chem., Int. Ed.*, 2016, **55**(15), 4729–4733.
40 M. M. Bordbar, A. Sheini, P. Hashemi, A. Hajian and H. Bagheri, Disposable paper-based biosensors for the point-of-care detection of hazardous contaminations-A review, *Biosensors*, 2021, **11**(9), 316.